International Journal of Mechanical, Industrial and Aerospace Sciences
ISSN: 2517-9950
Vol:6, No:3, 2012

Numerical Simulation of the Flow Field around a 30° Inclined Flat Plate

M. Raciti Castelli, P. Cioppa and E. Benini

***Abstract*—**This paper presents a CFD analysis of the flow around a 30° inclined flat plate of infinite span. Numerical predictions have been compared to experimental measurements, in order to assess the potential of the finite volume code of determining the aerodynamic forces acting on a flat plate invested by a fluid stream of infinite extent.

Several turbulence models and spatial node distributions have been tested and flow field characteristics in the neighborhood of the flat plate have been numerically investigated, allowing the development of a preliminary procedure to be used as guidance in selecting the appropriate grid configuration and the corresponding turbulence model for the prediction of the flow field over a two-dimensional inclined plate.

***Keywords*—**CFD, lift, drag, flat plate

I. Introduction

THE flow field around bluff bodies has been extensively studied, due to its relevance to drag on vehicles, ship hulls and submarines. Such flows provide rich and interesting fluid dynamics of considerable engineering relevance. Bluff bodies such as plates, discs, circular and rectangular cylinders and V-shaped prisms are used in combustors to enhance scalar mixing and to provide a flame-stabilizing region [1]. They are also adopted in air diverters, enabling hovercraft fans to determine both vertical and horizontal thrusts [2] [3]. Several investigations on some classical configurations have been done, both experimentally and numerically, in order to understand the fundamental aspects of wakes and flow-induced vibration.One of the earliest works about vortex shedding from a sharp-edged plate was performed by Fage and Johansen [4], who analyzed the flow field around a flat plate for 18 different angles of incidence. Jackson [5] simulated the periodic behavior of a two-dimensional laminar flow past various shaped bodies, including flat plates aligned over a range of angles of attack with respect to the incoming free-stream. Knisely [6] performed Strouhal number measurements of several rectangular cylinders with side ratios ranging from 0.04 to 1.0 and with angles of attack ranging from 0° to 90°.

Marco Raciti Castelli is a Research Associate at the Department of Industrial Engineering of the University of Padova, Via Venezia 1, 35131 Padova, Italy (phone: 0039-3207179239; e-mail: marco.raciticastelli@unipd.it).

Paolo Cioppa is a M.Sc. Student in Aerospace Engineering at the Department of Industrial Engineering of the University of Padova, Via Venezia 1, 35131 Padova, Italy.

Ernesto Benini is an Associate Professor at the Department of Industrial Engineering of the University of Padova, Via Venezia 1, 35131 Padova, Italy (e-mail: ernesto.benini@unipd.it).

Lam [7] investigated the flow past an inclined flat plate at α=15°, using phased-averaged LDA measurements.

The flow field around flat plates, characterized by sharp leading and trailing edges, was also investigated by Breuer and Jovicic [8].

Breuer et al. [9] simulated the flow over an 18° inclined plate, showing how the trailing edge vortices are able to dominate the wake features.

Zhang et al. [10] studied the transition route from steady to chaotic state for a flow around an inclined flat plate.

The present investigation focuses on the numerical analysis of the flow around a 30° inclined flat plate of infinite span. A full campaign of CFD simulations was performed, in order to investigate the effect of different spatial grid resolutions and turbulence models on the capability of the numerical code of reproducing the experiments of Fage and Johansen [4]. The normal force coefficient was numerically determined, as well as the velocity distributions over both the leading edge and the trailing edge of the plate, allowing the development of a preliminary procedure to be used as a guidance for future numerical works.

II. The Case Study

Fage and Johansen measurements [4] were performed on a flat, sharp-edged rectangular steel plate, whose main dimensions are reported in Table I.

TABLE I
Main geometrical features of the vertical flat plate adopted by Fage and Johansen (From: [4])

Denomination	Value [m]
l	2.1336
b	0.1511
s	0.0045

The cross-section of the plate, normal to the span, is shown in Fig.1. In order to avoid plate deflection, the frontal surface was flat and the rear one resulted slightly tapered from the centre, where the thickness reached 3% of the chord value, towards the sharp edges. The forces on the plate, inclined at various angles to the wind, were estimated for two-dimensional flow, from pressure measurements taken in the median section. The pressure distribution over the front surface was measured at an unperturbed wind speed of 15.25 m/s.

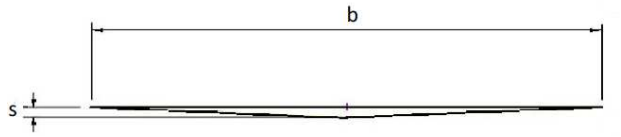

Fig. 1 Cross section of the flat plate, normal to the span

The values of the normal force coefficient k_N, defined as:

$$k_N = F_N / (b\rho V_0^2) \quad (1)$$

were estimated from the pressure coefficients along the plate, in formulas:

$$c_p = (p - p_0)/\rho V^2 \quad (2)$$

The measured values of k_N are given in Table II (2nd column).

TABLE II
MEASURED VALUES OF K_N FOR DIFFERENT PLATE INCLINATION ANGLES (FROM: [4]). THE RED RECTANGLE EVIDENCES THE REFERENCE DATA ADOPTED FOR PRESENT COMPUTATIONS

α°	k_N. Wind tunnel. (A)	k_N. Kirchhoff-Rayleigh. (B)	k_N. Ratio of wind-tunnel k_N to theoretical k_N. (C)	Wind-tunnel values of $(p_m - p_0/\rho V_0^2)$ (D)	$(V_1/V_0)^2$. (E)
0	0	0	—	—	—
3	0·165	0·040	4·10	—	—
6	0·345	0·075	4·60	—	—
9	0·445	0·110	4·05	—	—
15	0·425	0·170	2·50	—	—
20	0·470	0·215	2·20	—	—
30	0·645	0·280	2·30	−0·462	1·92
40	0·785	0·335	2·35	−0·544	2·09
50	0·900	0·375	2·40	−0·615	2·23
60	0·985	0·405	2·45	−0·664	2·33
70	1·035	0·425	2·45	−0·680	2·36
80	1·060	0·435	2·45	−0·688	2·38
90	1·065	0·440	2·45	−0·690	2·38

III. Spatial Domain Discretization

All the meshes adopted in the present work had common geometric features, except for the areas close to the flat plate. Inlet and outlet boundary conditions were placed respectively 12 chords upwind and 25 chords downwind with respect to the plate, allowing a full development of the wake.

The discretization of the computational domain into macro-areas led to two distinct sub-grids:

- a rectangular outer zone, determining the overall calculation domain, with a circular opening centered on the flat plate;
- a circular inner zone, containing the vertical flat plate.

The circular inner zone had no physical significance: its aim was to allow a precise dimensional control of the grid elements in the area close to the flat plate by adopting a first size function, operating from the plate to the control circle itself, and a second size function, operating from the control circle to the whole computational domain.

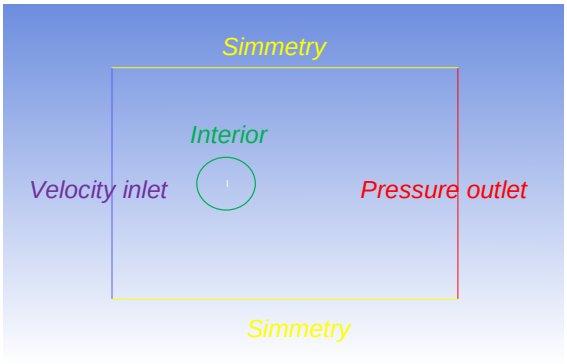

Fig. 2 Boundary conditions of the computational domain

TABLE III
MAIN GEOMETRICAL FEATURES OF MOD1 GRID

Denomination	Value
Uniform grid spacing on the flat plate [mm]	1
Growth factor from the flat plate to the control circle [-]	1.1
Maximum grid dimension inside the control circle [mm]	5
Maximum grid spacing inside the computational domain [mm]	100

TABLE IV
MAIN GEOMETRICAL FEATURES OF MOD2 GRID

Denomination	Value
Uniform grid spacing on the flat plate [mm]	1.5
Growth factor from the flat plate to the control circle [-]	1.1
Maximum grid dimension inside the control circle [mm]	5
Maximum grid spacing inside the computational domain [mm]	100

TABLE V
MAIN GEOMETRICAL FEATURES OF MOD3 GRID

Denomination	Value
Uniform grid spacing on the flat plate [mm]	2
Growth factor from the flat plate to the control circle [-]	1.1
Maximum grid dimension inside the control circle [mm]	5
Maximum grid spacing inside the computational domain [mm]	100

TABLE VI
MAIN GEOMETRICAL FEATURES OF MOD4 GRID

Denomination	Value
Uniform grid spacing on the flat plate [mm]	4
Growth factor from the flat plate to the control circle [-]	1.1
Maximum grid dimension inside the control circle [mm]	10
Maximum grid spacing inside the computational domain [mm]	100

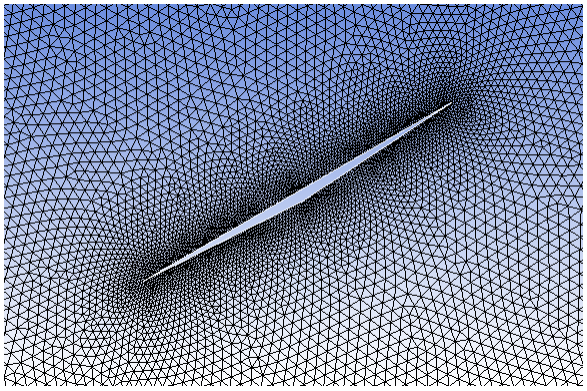
Fig. 3 Near-plate grid distribution, MOD1

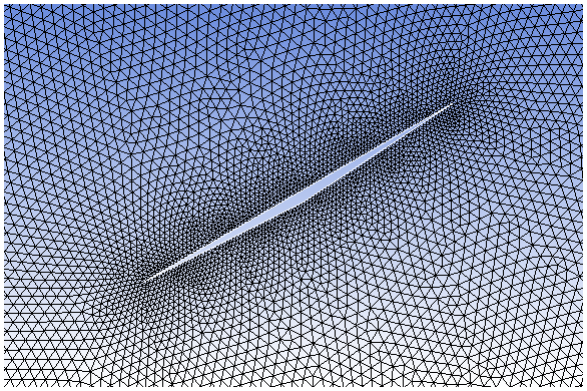
Fig. 4 Near-plate grid distribution, MOD2

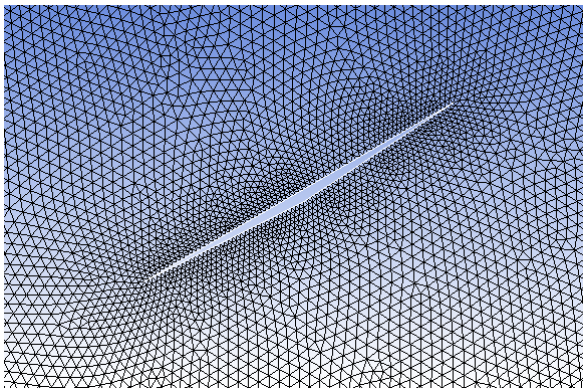
Fig. 5 Near-plate grid distribution, MOD3

Two *Symmetry* boundary conditions were adopted for the two side walls. The circumference around the circular opening, centered on the flat plate, was set as an *Interface*, thus ensuring the continuity of the flow field. Fig. 2 shows the boundary conditions of the computational domain.An unstructured mesh was chosen, in order to reduce engineering time to prepare the CFD simulations and also in order to test the prediction capability of a very simple grid. Considering their features of flexibility and adaption capability, unstructured meshes are in fact very easy to obtain, also for complex geometries, and often represent the “first attempt” to get a quick response from the CFD in engineering work.

In order to test the numerical code sensitivity to grid resolution, four different near-plate meshes were analyzed in the present work. Tables from III to VI show the main features of the adopted grid architectures, which are also reproduced in Figs. from 3 to 6, while Fig. 7 displays a view of the grid of the whole computational domain, showing also the control circle.

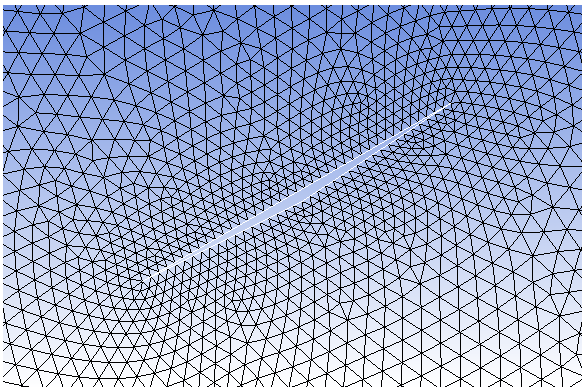
Fig. 6 Near-plate grid distribution, MOD4

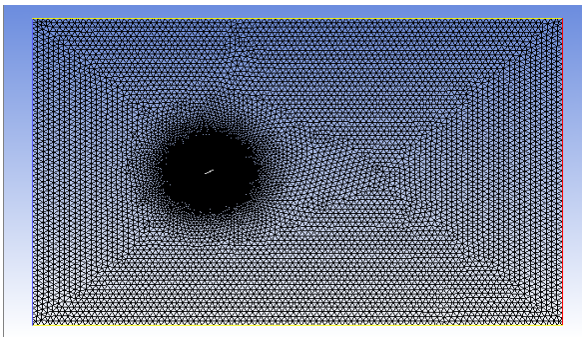
Fig. 7 View of the whole computational domain grid distribution, MOD2

IV. Turbulence Models and Convergence Criteria

The CFD software Ansys Fluent ® was adopted to numerically determine the surface pressure distribution on the vertical flat plate. Through its integration along the upwind and downwind faces of the flat plate, a net force vector was obtained. Calculations were completed using the following turbulence models:

- *Standard k-ε*, using the *Standard Wall Functions* (*SWF*) option;
- *Realizable k-ε*, using the *Standard Wall Functions* (*SWF*) option;
- *Realizable k-ε*, using the *Non-Equilibrium Wall Functions* (*NEWF*) option;
- *NRG k-ε*.

Calculations were run until small residuals were obtained ($\sim 10^{-5}$). Each simulation, performed on a 2.33 GHz clock frequency quad core CPU with Hyper-Threading, required a total computational time of about 2 hours.

V. Results and Discussion

Fig. 8 represents a comparison between experimentally measured (from: [4]) and numerically predicted normal force coefficients as a function of both grid spacing and turbulence models. As can be clearly seen, the best results were registered for *Realizable k-ε* turbulence model, adopting the *SWF* option, and MOD2 grid spacing.

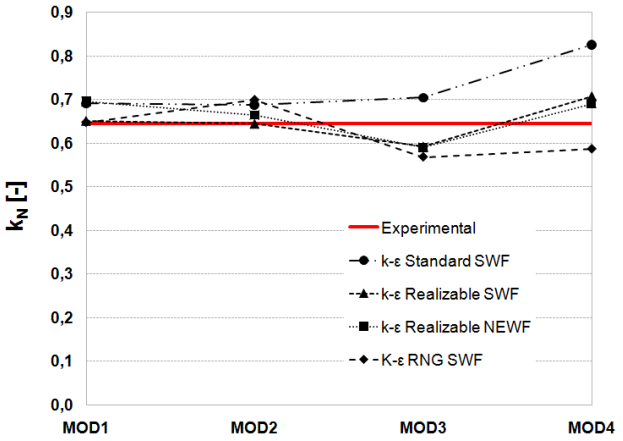

Fig. 8 Comparison between measured (from: [4]) and numerically predicted normal force coefficients

TABLE VII
Resulting normal force coefficients and relative deviations with respect to experimental data, Standard k- ε SWF

Mesh denomination	k_N [-]	Δk_N [%]
MOD1	0.691	7.16
MOD2	0.688	6.68
MOD3	0.705	9.29
MOD4	0.826	28.08

TABLE VIII
Resulting normal force coefficients and relative deviations with respect to experimental data, Realizable k- ε SWF

Mesh denomination	k_N [-]	Δk_N [%]
MOD1	0.651	0.90
MOD2	0.644	-0.15
MOD3	0.592	-8.21
MOD4	0.707	9.66

TABLE IX
Resulting normal force coefficients and relative deviations with respect to experimental data, Realizable k- ε NEWF

Mesh denomination	k_N [-]	Δk_N [%]
MOD1	0.696	7.91
MOD2	0.664	2.97
MOD3	0.590	-8.50
MOD4	0.690	7.04

The resulting normal force coefficients and their deviations with respect to the experimental data, in formulas:

$$\Delta k_N = [(k_{N,numerical} - k_{N,experimental})/k_{N,experimentral}]\cdot 100 \quad (3)$$

are summarized in Tables from VII to X.

TABLE X
Resulting normal force coefficients and relative deviations with respect to experimental data, RNG k- SWF

Mesh denomination	k_N [-]	Δk_N [%]
MOD1	0.648	0.42
MOD2	0.699	8.44
MOD3	0.568	-11.93
MOD4	0.587	-9.06

The investigation of the flow field across the inclined flat plate continued through the exploration of the velocity profiles across the boundaries of the dead-air region, along a line normal to the edge and the undisturbed wind direction at several distances (reported in Table XI) behind the plate, as represented in Fig. 9.

TABLE XI
Distance of the vertical measurement lines from the leading and trailing edges of the flat plate

Denomination	x_i [m]	y/b [-]
T.E.	0.0704	0.24 ÷ 0.38
L.E.	-0.0604	-0.24 ÷ -0.38

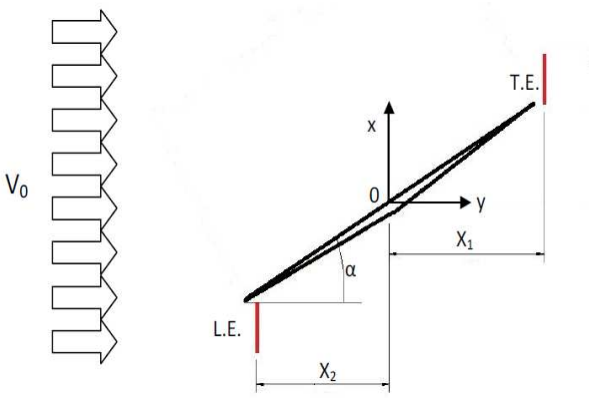

Fig. 9 Vertical measurement lines close to the leading and trailing edges of the flat plate

The comparison between experimental measurements and numerical predictions is summarized by Figs. 10 and 11. The sudden increase of velocity across the dead-air boundary at each edge of the plate is clearly visible. It can also be noticed that the numerical code is able to correctly reproduce this phenomenon, as can be seen also from Fig. 12, showing the absolute pathlines across the analyzed flat plate.

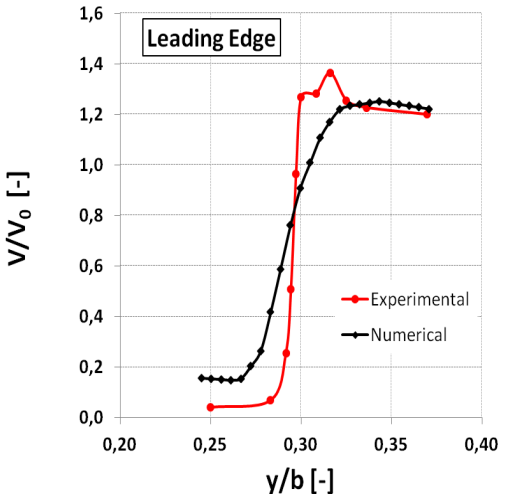

Fig. 10 Comparison between experimentally measured (from: [4]) and numerically predicted normalized velocities across the leading edge of the flat plate

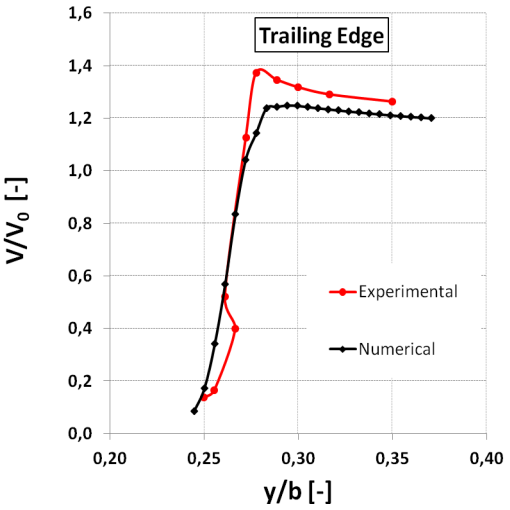

Fig. 11 Comparison between experimentally measured (from: [4]) and numerically predicted normalized velocities across the trailing edge of the flat plate

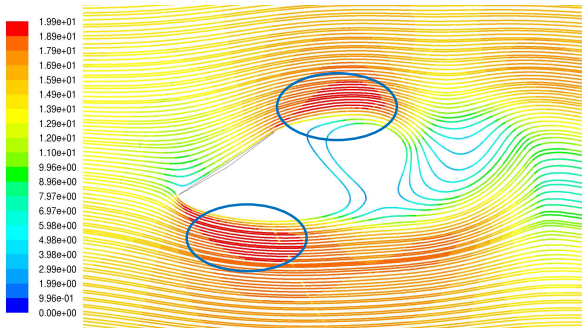

Fig. 12 Visualization of the sudden increase of absolute velocity across the dead-air boundaries at each edge of the inclined plate (evidenced by the blue circles) through the plot of the absolute pathlines, colored by particle velocity [m/s]

VI. Conclusions and Future Work

A CFD analysis of the flow field around a thin flat plate of infinite span, inclined at 30° to a fluid stream of infinite extent, was presented. Numerical predictions were compared to experimental measurements, in order to assess the potential of the finite volume code of determining the aerodynamic forces acting on a bluff body invested by a fluid stream.

Several turbulence models and spatial node distributions were tested. *Realizable k-ε* turbulence model, adopting the *SWF* option, proved to be the best choice. The numerical code prediction capabilities proved to be good, being the experimental normal force coefficient underestimated of the 0.15% (for the chosen set-up of spatial grid distribution and turbulence model).

The numerical code capabilities to predict the rapid increase of velocity across the dead-air boundaries at each edge of the flat plate resulted quite good, being numerically computed velocities very similar to experimental measurements.

Nomenclature

b [m]	flat plate chord
c_p [-]	pressure coefficient
F_N [N]	normal force per unit length of the plate
l [m]	plate length in the span-wise direction
k_N [-]	normal force coefficient
$k_{N,experimental}$ [-]	measured normal force coefficient
$k_{N,numerical}$ [-]	computed normal force coefficient
p [Pa]	static pressure
p_0 [Pa]	static pressure of the unperturbed free-stream
s [m]	plate thickness
V [m/s]	air velocity
V_0 [m/s]	unperturbed air velocity
x_i [m]	distance of the measurement lines from the leading and trailing edges of the plate (i=1,2,3)
y [m]	vertical distance from the edge of the flat plate
y/b [-]	normalized vertical distance from the edge of the flat plate
Δk_N [%]	deviation of the numerically predicted normal force coefficient with respect to the experimental data
μ [Pa·s]	air dynamic viscosity (assumed $1.789 \cdot 10^{-5}$)
ρ [kg/m^3]	unperturbed air density (assumed 1.225).

Acknowledgment

The present work was funded by the EU FP7 Hoverspill project, Multi Environment Air Cushion Oil Spill Fast Response & Post Emergency Remediation System, Grant No. 234209.

References

[1] M. Breuer and N. Jovicic, "Separated flow around a flat plate at high incidence: an LES investigation", *Journal of Turbulence*, Volume 2, Issue 1, pp. 018 (2001).

[2] A. Kasniunas, T. Robertson and Z. Howe, *Hovercraft*, Rose-Hulman Institute of Technology, Terre Haute (Indiana), 2007.
[3] R. Yoshida, T. Yamamura and K. Kadota, "Propulsive Air Stream Deflecting Apparatus for Air Cushion Vehicle", *United States Patent No. 5,007,495*, Issued on Apr. 16, 1991.
[4] A. Fage and F. C. Johansen, "On the flow of air behind an inclined flat plate of infinite span", *Brit. Aero. Res. Coun. Rep. Memo. 1104*, pp. 81-106 (1927).
[5] C. P. Jackson, "A finite-element study of the onset of vortex shedding in flow past variously s,haped bodies", J. Fluid Mech., Volume 182, pp. 23-45 (1987).
[6] C. W. Knisely, "Strouhal numbers of rectangular cylinders at incidence: a review and new data" *J. Fluid Structures*, Volume 4, pp. 371-393 (1990).
[7] K. M. Lam, "Phase-locked eduction of vortex shedding in flow past an inclined flat plate", *Phys. Fluids*, Volume 8, pp. 1159-1168 (1996).
[8] M. Breuer and N. Jovicic, "Separated flow around a flat plate at high incidence: an LES investigation", *Journal of Turbulence*, Volume 2, pp. 1-15 (2001).
[9] M. Breuer, N. Jovicic and K. Mazaev, "Comparison of DES, RANS and LES for the separated flow around a flat plate at high incidence" *Int. J. Num. Meth. Fluids*, Volume 41, pp. 357-388 (2003).
[10] J. Zhang, N. S. Liu and X. Y. Lu, "Route to a chaotic state in fluid flow past an inclined flat plate", *Phys. Review*, E. 79, pp. 045306: 1-4 (2009).